Matveev Alex (Orcid ID: 0000-0003-4103-9131)

Winter Accumulation of Methane and its Variable Timing of Release from Thermokarst Lakes in Subarctic Peatlands

Alex Matveev[1,2,3], Isabelle Laurion[1,4], and Warwick F. Vincent[1,2,3]

[1]Centre for Northern Studies (CEN), Québec, QC, Canada.

[2]Département de biologie, Université Laval, Québec, QC, Canada.

[3]Takuvik Joint International Laboratory (CNRS-Université Laval), Québec, QC, Canada.

[4]Centre Eau Terre Environnement, Institut national de la recherche scientifique, Québec, QC, Canada.

Running title: winter methane in thermokarst lakes

Corresponding author: Alex Matveev (alex.matveev.1@ulaval.ca)

Key Points:

- Peatland permafrost lakes are ice-covered for more than half the year, and dissolved oxygen is undetectable in the underlying waters through most of this time
- Large amounts of dissolved methane build up in winter, which likely results in high methane efflux rates to the atmosphere during ice break-up in spring
- Lakes with low fetch to depth ratios may not release their bottom water methane to the atmosphere until fall convective mixing

This article has been accepted for publication and undergone full peer review but has not been through the copyediting, typesetting, pagination and proofreading process which may lead to differences between this version and the Version of Record. Please cite this article as doi: 10.1029/2019JG005078

Abstract Previous studies of thermokarst lakes have drawn attention to the potential for accumulation of CH_4 under the ice and its subsequent release in spring, however such observations have not been available for thermokarst waters in carbon-rich peatlands. Here we undertook a winter profiling of five black-water lakes located on eroding permafrost peatlands in subarctic Quebec for comparison with summer profiles, and used a two-year dataset of automated water temperature, conductivity and oxygen measurements to evaluate how the annual mixing dynamics may affect the venting of greenhouse gases to the atmosphere. All of the sampled lakes contained large amounts of dissolved CH_4 under their winter ice cover. These sub-ice concentrations were up to five orders of magnitude above air-equilibrium (i.e., the expected concentration in lake water equilibrated with the atmosphere), resulting in calculated emission rates at ice break-up that would be 1-2 orders of magnitude higher than mid-summer averages. The amount of CO_2 dissolved in the water column was reduced in winter, and the estimated ratio of potential diffusive CO_2 to CH_4 emission in spring was half the measured summer ratio, suggesting a seasonal shift in methanogenesis and bacterial activity. All surface lake ice contained bubbles of CH_4 and CO_2, but this amounted to <5% of the total amount of the dissolved CH_4 and CO_2 in the corresponding lake water column. The continuous logging records suggested that lake morphometry may play a role in controlling the timing and extent of CH_4 and CO_2 release from the water column to the atmosphere.

Plain Language Summary

Waterbodies that are formed by the thawing and collapse of ice-rich permafrost ('thermokarst lakes') are known to be major sources of greenhouse emissions in northern landscapes, but the seasonal variation in these emissions is not well understood. In this study, we measured the concentrations of methane and carbon dioxide beneath the ice of five thermokarst lakes in late winter, and compared these with summer concentrations and profiles. These 'black-water lakes' are located in subarctic peatlands, and are darkly colored because of their high concentrations of permafrost-derived, colored organic carbon. The results showed a winter accumulation of gases beneath the ice that would result in 10 to 100 times greater emissions from the surface waters at spring ice break-up than during summer open water conditions. However, continuous in situ measurements of water temperature and oxygen showed that lakes with smaller area to depth ratios may partially retain greenhouse gases that accumulated in their bottom waters throughout winter, thereby limiting the loss of methane in spring that would otherwise occur. More complete mixing occurred during fall cooling and circulation, and release of gases accumulated in the bottom waters during winter and summer may occur at that time. The exact volume of lake water that is mixed during the spring and fall periods is likely related to the wind fetch and depth of the basin. These results underscore the need for improved all-season measurements of greenhouse gas accumulation and emissions, particularly during the shoulder periods immediately before and after the period of winter ice-cover.

1. Introduction

Thermokarst lakes occur in high abundance across the Arctic and collectively account for 200,000 to 350,000 km^2 of open water in summer (Grosse et al., 2013; Olefeldt et al., 2016). These lakes have an increasing positive feedback effect on climate associated with permafrost thawing and the mobilization of soil carbon stocks (Vincent et al., 2013; Grosse et al., 2016; Chaudhary et al. 2017). Although the methane-emitting nature of thermokarst lakes has been well established over the last 20 years (Zimov et al., 1997; Vonk et al., 2015), the high spatial and temporal variability of such emissions remains little explored (Negandhi et al., 2013; Schneider von Deimling et al., 2015). These uncertainties have led to a limited representation of the Arctic greenhouse gas (GHG) fluxes in general circulation models, as well as to large uncertainties in regional and global estimates of carbon sources and sinks (Abnizova et al., 2015; Grosse et al., 2016; Schneider von Deimling et al., 2015). An improved understanding of the variability of GHG emissions associated with thermokarst lakes in different types of landscapes will allow for the development of improved process-based models (Saunois et al., 2016), more detailed parameterization of climate models (Chadburn et al., 2017), and ultimately for improved estimates of the Arctic GHG balance.

Thermokarst lakes vary greatly in their geomorphological characteristics (Livingstone et al., 1958; Olefeldt et al., 2016), limnology (Breton et al., 2009; Wrona et al., 2016), optical properties (Watanabe et al., 2011; Wauthy et al., 2018), and in GHG emission rates (Laurion et al., 2010; Grant et al., 2015; Wik et al., 2016a). Extensive research has been conducted on thermokarst lakes in the Pleistocene-aged ice-rich yedoma permafrost regions (e.g., Zimov et al., 1997; Arp and Jones, 2009; Morgenstern et al., 2011; Grosse et al., 2013; Schirrmeister et al., 2013). Thermokarst lakes in other, non-yedoma permafrost regions have been little studied to date, yet these are estimated to contain about 75% of the global permafrost carbon (Vonk et al., 2015). One such category is thermokarst lakes on organic-rich peatlands.

Peatland lakes in general are known to be large CH_4 emitters (Wik et al., 2016a), and in permafrost regions, peatland thermokarst lakes are known to release more methane than most other thermokarst lake types (Matveev et al., 2016).

The uncertainty in overall magnitude of thermokarst GHG fluxes to the atmosphere is the result of a scarcity of observations (Powers and Hampton, 2016), the poorly understood seasonality of thermokarst lakes (Holgerson and Raymond, 2016), and large differences in emission rates observed among the lakes studied to date (Vonk et al., 2015). The majority of thermokarst lakes are located in regions with limited access for ground observations, particularly during the period of winter snow-cover (Jones et al., 2011; Arp et al. 2016). As a result, the data on GHG dynamics in thermokarst lakes are mostly limited to the open-water season (Hampton et al., 2017; Wik et al., 2016b). The importance of obtaining multi-seasonal observations on these lakes is well recognized (Utsumi et al., 1998; Hampton et al., 2015; Denfeld et al., 2018), especially for the winter period that favors anoxic conditions and methanogenesis, with dampened or suppressed rates of methane oxidation (Ricão Canelhas et al., 2016). Previous studies of subarctic thermokarst lakes, including those in peatland thermokarst regions, have shown that these lakes may have prolonged periods of anoxia that are conducive to methane production (Deshpande et al., 2015, Matveev et al. 2018). Methane can accumulate in ice-capped lakes in concentrations surpassing those at open-water periods (MacIntyre et al. 2018; Cunada et al. 2018), with a potential outburst of gas at ice-out (Michmerhuizen et al. 1996, Jammet et al. 2017, Denfeld et al. 2018).

In the present study, we aimed to evaluate the winter characteristics of a set of peatland thermokarst lakes. Specifically, our objectives were to: (1) quantify their capacity for storing CH_4 and CO_2 under the seasonal lake ice; and (2) evaluate the potential for release of these gases to the atmosphere with wind-driven and convective lake mixing, particularly at the spring break-up of the ice and during autumnal overturn. We measured vertical profiles of

both gases in five subarctic peatland thermokarst lakes during winter, evaluated the seasonal changes in gas distribution relative to new and published summer profiles, measured the variations in underwater temperature, conductivity and oxygen with automated loggers, and continuously tracked the dynamics of ice cover with automated cameras. The fetch and depth variations among these lakes also allowed consideration of the effects of basin morphometry on the timing of gas emissions.

2. Materials and Methods

2.1. Study sites and sampling

The study region is within the sporadic (< 2% of the total land surface) permafrost zone of subarctic Quebec, Canada. The lakes are located in two peatland valleys, 3 km south (SAS1) and 0.5 km north (SAS2) of the Sasapimakwananisikw River, around 10 km southwest of Whapmagoostui-Kuujjuarapik (Table 1). A site location map is given in Supporting Information Figure S1 and landscape features are shown in Figure 7 of Vincent et al. (2017). The lakes occur alongside organic-rich palsa mounds (organic-rich hillocks with ice-rich permafrost cores) that hold most of the remaining permafrost in the region. The valleys contain around one hundred palsa mounds that are 3 to 5 m high and sparsely covered by lichens and shrubs (Filion et al., 2014, Matveev et al., 2016). Most of the palsas have 1 to 4 m deep thermokarst lake at their base resulting from the degradation of ice-rich permafrost, which started around 150 yr BP (Bhiry et al., 2012). Due to erosion of organic-rich palsas (Deshpande et al., 2016), the lakes contain high concentrations of terrestrially derived humic materials (Wauthy et al., 2018) and are darkly colored (deep brown and black), with limited water transparency. Semi-aquatic plants occur around the edge of the lakes, predominantly *Carex rariflora*, *Carex aquatilis* and *Eriophorum angustifolium*.

The late winter sampling campaign in the two valleys took place from 18 to 25 March 2016 (Table 2). Each of the five lakes was partially cleared of snow cover (0.6-0.8 m deep), and a hole was drilled through the lake ice (0.5 – 0.6 m deep) close to the maximum depth point. Triplicate samples were then collected for dissolved gas analyses (section 2.5).

Sampling was also conducted in late summer during the open water conditions (total of 155 summer dissolved gas samples (2012-2015) in the SAS valley lakes; the full dataset is archived in Matveev et al., 2019). Additionally, two moorings with automated sensors were deployed over 12-month period (including the winter sampling visit), in the deep central part of lakes SAS1A and SAS2A from Aug 2014 to Aug 2015 (details given in Deshpande et al. 2017, and data replotted in this paper as a comparison), and lakes SAS2A and SAS2C from Aug 2015 to Aug 2016 (section 2.4).

2.2. Lake surface imagery

Surface observations at two sites were taken continuously from 2014 to 2016 with automated cameras (Reconyx PC800, Holmen, WI, U.S.A.). These were positioned 5-10 m from the edge of lakes SAS1A and SAS2A. Six photographs were taken each day at 1 h intervals between 10:00 h and 15:00 h (Eastern Standard Time), and the records were retrieved annually each August. The complete dataset is archived in the Nordicana D data repository (Pienitz et al., 2017). The camera records were also used to monitor the thickness of the snow cover relative to a water level pole installed at the edge of each lake (Figure S2). The snow depth estimates were further validated in situ during the winter sampling visit.

2.3. Weather and climate data

Surface air temperature at SAS1 and SAS2 sites was recorded continuously by the automated cameras (Reconyx PC800, Holmen, WI, U.S.A.), while air and ground temperatures, solar radiation, wind speed and wind direction were collected from the SILA

meteorological station of the CEN research station at Whapmagoostui-Kuujjuarapik. Surface air temperatures, wind speed, wind direction, and atmospheric pressure were also measured in situ at each site during the visits with a portable weather probe (Kestrel 4500, Nielsen-Kellerman Co. Boothwyn, PA), and the data used to validate the continuous measurements at the meteorological station.

2.4. Limnological sampling

Water thermal structure, dissolved oxygen and conductivity were measured continuously throughout the year with automated loggers installed in SAS1A (2014-2015), SAS2A (2014-2016) and SAS2C (2015-2016), while water column profiling during visits in July-August (2013-2016) and March (2016) provided a suite of limnological observations from all studied lakes (Supporting Information Table S1). Data from all loggers were read immediately upon returning to the field station lab, with the exception of one faulty RBRsolo T from SAS2C at 2.1 m; the 2.25 m temperature record from the two other instruments was used in the analysis instead. No significant biofouling on any sensors was observed.

2.5. CH_4 and CO_2 concentrations

Under-ice CH_4 and CO_2 profiles were obtained from the five lakes during the late winter (March 2016) field campaign. The lakes were sampled through the holes in the ice with a custom-built thin-layer sampler (Supplemental Information Figure S3) connected to a peristaltic pump (MSP250, Manning Env., Inc. Georgetown, TX, USA; flow rate of 927 mL min^{-1}). The dissolved gases were extracted from the lake water samples using the headspace method (Supporting Information Table S1). A heated shelter with access to the ambient air was used to prevent water from freezing during the gas extraction procedure. The gas samples were stored at higher pressure than ambient to facilitate sampling for gas chromatography: 10 mL of sample were injected into 5.9 mL Labco Exetainer® vials (Labco Limited, UK) that had been previously flushed with N_2 and vacuumed. Samples were also

collected with the thin-layer sampler during the open water period in July – August (2013-2016) and processed following the above procedures. Dissolved CH_4 and CO_2 concentrations in the gaseous samples were measured by gas chromatography using a Thermo 1310 GC equipped with a TRI-Plus Head-Space auto-sampler, two columns in series, HSQ 80/100 4×1/16" and MS 5A 6×1/16", a thermal conductivity detector and a flame ionization detector.

Gas concentrations in lake ice were measured in melt water from the top 0.3 m of the ice, using a technique similar to that described in Langer et al. (2015). The ice blocks were cut from the top of the lake ice cover down to 0.4 m deep, and transferred to the station. Ice cubes of ca. 1.5 L volume were then cut from the larger blocks near the middle part of the lake-ice column (total ice depth ca. 0.6 m), and immediately sealed in pre-evacuated double-walled plastic bags (CTI Industries Corp., Canada). The bags were then vacuumed to 0.3–0.4 Torr with a vacuum pump (Gast High-Capacity Vacuum/Pressure Pump), and left at room temperature to melt the ice. Upon melting of the ice, the headspace was sampled and CH_4 and CO_2 concentrations measured by gas chromatography as above, considering the ice sample volume, temperature, and pressure. The total amount of dissolved gas in the total ice volume were then calculated for the measured ice depth, with the assumption that concentrations in the middle of the ice were representative of the entire ice column. All gas profiles and limnological data are available in Matveev et al. (2019).

3. Results

3.1. Climate

The mean annual air temperature (MAAT) measured by an automated weather station (KJRAPIK.site#2) in the SAS study region (about 8 km from the study sites) for the period from 29 Aug 2015 to 1 Sep 2016 (Figure 1) was –2.9 ºC (SD=13.3 ºC), which was 1.5 ºC above the multi-year (1971-2000) average of –4.4 ºC in this region (data by Environment

Canada); winter minimum and summer maximum values were –41.7 and 31.2 ºC, respectively (CEN, 2017). During the same period, air temperatures measured by the automated camera installed at lake SAS2A (in the SAS2 valley) varied from –42 ºC (12 Feb 2016) to 33 ºC (2 Aug 2016), while slightly cooler conditions were registered by the camera at lake SAS1A (in the SAS1 valley), ranging from –48 ºC (5 Jan 2015) to 29 ºC (29 Jul 2015). The wind speeds observed over SAS1 lakes during the visits were typically 1 to 10 % higher than over SAS2 lakes. The mean wind speed (U_{10}) measured at the automated weather station was 3.4 m s^{-1} (SD = 1.9 m s^{-1}), with maximum average wind speeds observed in the fall (October - December) of 2015 (Figure 1).

3.2. Ice and snow phenology recorded by the automated cameras

For SAS2A in 2015, the ice first covered the lake for two days on 12-13 Oct, and the onset of a persistent seasonal ice cover began on 18 Oct. The snow depth increased to 0.1 m above the lake ice by 1 Nov, and then continued to increase by about 0.1 m per month, until reaching 0.55 m depth by the end of March 2016. The snow depth began decreasing on 12 Apr, and dropped by 0.4 m before melting completely. Snowmelt increased the lake water level by ca. 0.15 m, until the end of June, when the water level dropped to the longer-term average. The ice first opened on 12 May, and the lake was clear of ice by 30 May 2016.

Similar variations were observed at SAS1A, but with the period of ice cover that started 1 day earlier and first opened 2 days earlier than at lake SAS2A. Ice formation was first observed at SAS1A on 12 Oct 2015, with the onset of full seasonal ice cover by 17 Oct. The snow began to accumulate on 24 Oct, and reached 0.1 m depth by 12 Nov, 0.2 m by 12 Jan, and 0.5 m by the end of March. The lake ice began to open up on 10 May, and full open water was first recorded on 25 May 2016.

The camera images during the freeze-up period and before snowfall were inspected for evidence of gas bubbles trapped in the ice. The images indicated the simultaneous

presence of up to 40 bubbles for the whole lake with an average diameter of ca. 150 mm under the first ice cover forming on SAS2A on 12 and 18 Oct 2015. Camera records also showed the presence of smaller bubbles of ca. 50 mm in diameter, with an average density of 2-3 bubbles per m^2 (Supporting Information Figure S2a). Close to 20 bubbles of 100 to 150 mm diameter were simultaneously observed under the first ice cover forming on SAS1A on 12, 18, 19 and 20 Oct 2015, together with ca. 1-2 smaller bubbles per m^2 (Figure S2b). The number and location of the observed bubbles varied between the images (in the hourly sequence). No evidence of sustained bubbling was observed further in the sequence of images, suggesting the absence of sustained point-bubbling gas sources, and that bubbling events (likely escaping from sediments) might be linked to atmospheric pressure and ice formation.

3.3. Snow and ice conditions at the time of winter sampling

The lakes from the two valleys had spatially homogeneous snowpacks in March 2016. The average snow depth over the lakes was similar between valleys and averaged 49 cm (± 1 cm) at SAS2 (three lakes) and 53 cm (± 1 cm) at site SAS1 (two lakes) (Table 2). Two lakes in the SAS2 valley (SAS2A and SAS2B) had a 6-7 cm deep layer of water-saturated snow at the base of their snow cover over the ice, making the snowpack heavier than the snow around the lakes. The ice depth was also similar between sites, averaging 57 cm (±1 cm) at SAS2 and 61 cm (± 4 cm) at SAS1.

When the central lake area (ca. 1.5 m^2) was cleared of snow for drilling and sampling, there was no evidence of large bubbles trapped in the ice. Similarly, we found no evidence of large bubbles in a larger transect area (1.3 × 12 m) that was cleared along the central part of lake SAS2C. However, the ice over all sampled lakes was stippled by white-colored inclusions (1-2 mm in diameter) in the brown-grey water ice (Figure 2), likely produced by small bubbles of trapped gas.

3.4. Seasonal dynamics of temperature and oxygen

Lake SAS2A showed vertical gradients in water column properties through most of the year, with a period of cooling and partial mixing during fall 2015 (Figure 3, top panel). The ice started to grow at the beginning of November, with temperatures below 0 °C at 0.25 m depth that persisted until the break-up of ice near the beginning of June. The water column below depths of 0.75 m remained in the liquid phase throughout the winter, with the maximum cooling depth of about 1 m at the time of ice break-up (mid-May). Bottom waters cooled to a minimum of 2.8 °C during the ice-covered period. Inverse thermal gradients (increased temperature with depth) persisted under the ice from November to late May, followed by a brief (9-10 days) mixing event at ice-out, which also appeared to be restricted to the upper 1.75 m. Warming then continued, with maximum temperature differences between the surface and bottom waters reached by mid-August.

Most of water column in SAS2A was anoxic for most of the year (Figure 3, bottom panels). The mid-October mixing event briefly (for less than a day) caused oxygenation of the bottom waters (depth = 2.6 m) to a maximum of 0.45 mg O_2 L^{-1}, while at the middle of the lake water column (1.25 m) oxygen levels increased to 4 mg L^{-1} during fall mixing period (mid-September to mid-October), and to 8 mg L^{-1} during the spring mixing (lasting ca. 9 days at this depth in late May). The bottom waters remained anoxic following the mid-October mixing event and throughout the rest of the study period. The bottom waters had salinities, measured by conductivity (Figure 3, bottom panel), that were 2-3 times greater than at 1.25 m (Figure 3, middle panel) throughout the year, indicating the effect of dilute salt concentrations on density gradients in these thermokarst waters (Deshpande et al., 2015). Similar dynamics were observed in lake SAS2C in the same valley (Supplemental Information figures S4, S5, S6), and in SAS2A on the previous year, while the water column of lake SAS1A was more oxygenated (see section 3.7).

3.5. Winter and summer profiles

The winter and summer profiling showed strong thermal gradients down the water column in all five of the lakes in both seasons, with an inverse profile of increasing temperature with depth in winter, and a continuous gradient of sharply decreasing temperature with depth in summer (Figure 4). The below-ice water column in all lakes in both SAS valleys was completely anoxic in mid-winter, while in summer, the surface waters were oxygenated to varying degrees, but to a maximum of 80% of air equilibrium.

The oxygen profiles showed declining values with depth in summer, reaching anoxic conditions at the depth of 1.1 m in lake SAS1A (i.e., leaving 35% of the deepest water column anoxic), and at about 0.6 m in lake SAS1B (leaving 60% of the deepest water column anoxic). In the SAS2 valley, anoxia was reached at about 0.6 m in lake SAS2B (75% of the water column anoxic), and at about 0.4 – 0.5 m in lakes SAS2A and SAS2C (more than 80% of the water column anoxic). Thus, the shallower lakes studied in SAS1 valley (Z_r=4.0 and 9.4) were oxygenated to a greater extent than deeper lakes studied in the SAS2 valley (Z_r=14.5, 16.1, 17.7).

The vertical profiles of CH_4 and CO_2 under the ice and during the open water period in summer are presented in Figure 4 (lakes SAS1A, SAS2A and SAS2C shown; see also Figure S4). High concentrations of dissolved gases were found in winter, with a relatively homogenous distribution throughout the water column below the ice. This contrasted with the summer gas distribution, which showed a one (CO_2) or two (CH_4) order-of-magnitude rise in concentrations in the bottom waters (i.e. below 1.1, 0.5 and 0.4 m respectively in SAS1A, SAS2A and SAS2C; Figure 4).

The winter GHG concentrations at all depths were above those measured in the surface waters during summer, but similar or below those measured at the bottom of the lakes in summer. The total amount of dissolved winter methane integrated over the entire offshore

water column (i.e., summed by stratum, per m^2) was similar or above the corresponding summer values, to a variable extent (Table 3). The greatest difference was in SAS1A, the lake with lowest relative depth (Table 1), in which the winter methane per m^2 was 388% above the summer value.

Conversely, the total amount of dissolved CO_2 in the unit water column was 30-60% below that in summer, with the exception of SAS1A (Table 3). As a consequence of these divergent responses between the two gases, the CO_2 to CH_4 molar ratio doubled from an average (SD) of 9.9 (3.5) in winter to 19.8 (4.7) in summer, and a paired t-test showed that this increase was highly significant ($t= 4.1$, $df = 4$, $p = 0.007$).

3.6. CO_2 and CH_4 trapped in the lake ice

Both gases were detected at concentrations above air-equilibrium in the lake ice (except for CH_4 in SAS1B ice), which likely adds to atmospheric emissions during ice melt in spring. However, these amounts of gas in ice were small relative to those in the water column, and ranged from < 1% to a maximum of 6.6% of the amount of dissolved gas in the corresponding winter water column (Table 4).

3.7. Potential fluxes of CO_2 and CH_4 during mixing

The high concentrations of CO_2 and CH_4 in the winter water column indicate the potential for large emissions during the seasonal ice break-up, but this depends on the extent of spring mixing. To investigate this question further, we examined the continuous limnological record from an earlier study of SAS1A and SAS2A (Deshpande et al., 2017), and replotted these data for comparable depths and on the same scale (Figure 5).

The complete mixing of the water column that was recorded in spring for SAS1A would have raised the surface concentrations to about 1350 µmol CO_2 L^{-1} and 318 µmol CH_4 L^{-1} as estimated from the measured water column values. These surface concentrations would

result in diffusion rates of 736 mmol CO_2 m^{-2} d^{-1} and 170 mmol CH_4 m^{-2} d^{-1}, These surface concentrations would result in diffusion rates of 736 mmol CO_2 m^{-2} d^{-1} and 170 mmol CH_4 m^{-2} d^{-1}, calculated using a diffusion model adjusted for low solubility gases as in Vachon et al. (2010), and for near-surface wind mixing as in MacIntyre et al. (2010). These values will potentially gradually decrease until the concentrations reduced to produce the fluxes measured during the open water period. These estimated spring efflux rates are equivalent to 13 to 180 times the summer CO_2 efflux rates and 14 to 170 times the summer methane flux rates (4 to 55 mmol CO_2 m^{-2} d^{-1} and 1 to 12 mmol CH_4 m^{-2} d^{-1}; Matveev et al., 2016). The continuous records indicated only a partial mixing of SAS2A in spring, to 1.75 m depth. This would result in surface concentrations of 2320 µmol CO_2 L^{-1} and 200 µmol CH_4 L^{-1}, producing diffusion fluxes of 1448 mmol CO_2 m^{-2} d^{-1} and 111 mmol CH_4 m^{-2} d^{-1}. These estimated spring efflux rates are equivalent to 6 to 36 times the summer CO_2 efflux rates and 10-110 times the summer methane flux rates (40-242 mmol CO_2 m^{-2} d^{-1} and 1-10 mmol CH_4 m^{-2} d^{-1}; Matveev et al., 2016).

4. Discussion

Our observations indicate that peatland thermokarst lakes have the capacity to store high concentrations of CH_4 under their seasonal ice cover. Overall, these data support the suggestion by Wik et al., (2016b) that current evaluations are likely to underestimate annual CH_4 emissions from thermokarst lakes by the omission of winter measurements, and our observations show that this is particularly the case for peatland thermokarst lakes, where quantities of dissolved gas accumulated in the unit water column in winter were up to 389%, but more generally 2-10%, above those in summer. Most importantly, ice-out in spring would expose the surface waters with high concentrations of CH_4 to the atmosphere, resulting in a short period of strong emission fluxes at that time. The sub-ice concentrations surpassed the

air-equilibrium average of 0.0042 µmol L^{-1} by 4-5 orders of magnitude (Figure 4), which would translate into early spring efflux rates that are one to two orders of magnitude above the summer efflux rates based on diffusion calculations, highlighting the need for direct measurements during the important, but logistically challenging, spring break-up period.

The methane concentrations in peatland permafrost lakes measured here, and the resultant efflux rates, are high relative to values recorded or estimated for other Arctic lakes. For example, in an analysis of four Arctic lakes in Alaska, highest annual methane rates were observed under the ice in April, with values averaging (SD) 26 (9) mmol CH_4 m^{-3} (Townsend-Small et al., 2017), well below the winter values of 160-318 mmol CH_4 m^{-3} measured in the SAS lakes during winter. The summer diffusive fluxes (measured by chambers) in the four Alaskan lakes ranged up to 0.86 mmol CH_4 m^{-2} d^{-1}, orders of magnitude below the estimated summer values from the SAS lakes. In the vast permafrost peatland region of the Western Siberian Lowlands, Serikova et al. (2019) recorded especially high carbon emissions in the shoulder seasons, with C fluxes in spring and autumn that were on average 2-times greater than during summer; ice-out emission rates were highly variable, ranging from 0.1 to 50 mmol CH_4 m^{-2} d^{-1} for lakes in sporadic and isolated permafrost regions, but consistently below the rates at ice-out that we estimate for the SAS peatland lakes. In a set of flux tower measurements for a lake in subarctic Sweden (Jammet et al., 2017), emission rates were minimal during ice cover in winter and maximal in spring; the spring values were around 7 mmol CH_4 m^{-3} d^{-1} , on average three times the rate in summer, but again orders of magnitude below the estimated SAS spring rates (but within the range for summer rates).

The peatland thermokarst lakes studied here also stored a substantial amount of CO_2 in their waters under the ice (average of 2585 mmol m^{-2}, but with large variations among lakes). However, this was less than the corresponding amount of CO_2 accumulated in

summer, which on average was about 30% greater, resulting in a much higher ratio of diffusive CO_2 to CH_4 flux in summer. This may be an indication of the predominance of hydrogenotrophy and use of CO_2 for methanogenesis in these fully anoxic environments during the winter ice cover period (consistent with metagenomic observations of abundant hydrogenotrophic Methanomicrobiales in these waters in winter; Vigneron et al., 2019), followed by increased respiration by aerobic bacteria in summer accompanied by the methanotrophic oxidation of CH_4 (Crevecoeur et al., 2015). In addition, the lake ice stored both CH_4 and CO_2, in quantities of up to 5% of the water column quantities.

Our winter 2016 sampling revealed that 2 out of 3 lakes in the SAS2 region were susceptible to ice-fracturing in the winter, possibly by contraction cracks combined with the added weight of the snow. This resulted in the presence of liquid water in the basal 5-7 cm of the snow overlying the lake ice. Given that this lake water was highly saturated in CH_4 and CO_2, there would be gas emission events from this phenomenon during the ice cover period.

Our second set of questions related to the timing and extent of release of these GHGs to the atmosphere at spring break-up versus autumnal overturn. Previous studies of thermokarst lakes elsewhere indicated that dissolved gas accumulated during winter would be largely released during spring mixing, immediately after ice-out (Karlsson et al. 2013). However, the continuous data from SAS2A and SAS2C showed persistent gradients throughout the year, and incomplete mixing in either spring or fall. This stratification limits the extent of methane emission during summer; bottom-water accumulation of CH_4 in this lake would only be brought to the surface and released to the atmosphere during years of extreme cooling and mixing.

As in 2015/16, the 2014/15 data for SAS2A showed two periods of mixing: fall and spring. However, the spring mixing was mostly limited to two brief episodes during periods of higher winds and falling temperatures, while fall mixing occurred continuously over a

period of several weeks of cooling air and lake temperatures. Both lakes showed strong water column gradients in summer, with only a thin layer (< 25% of the total water column) of oxygenated waters at the surface, where methane concentrations were likely reduced as a result of evasion to the atmosphere, methanotrophy and less net release of methane into the water from the shallow oxygenated sediment. Each lake experienced anoxic conditions throughout the year, conducive to CH_4 and CO_2 accumulation. In the winter, under the 0.5–0.6 m of ice cover, anoxia rapidly extended throughout their entire volumes, providing conditions that were favorable for methanogenesis, and probably less favorable for methanotrophy.

Despite similarities in these general features, there were striking differences between SAS2A and SAS1A. Both lakes showed prolonged fall mixing, but there was much greater equilibration with the atmosphere in SAS1A, with oxygen values reaching near 100% of air-equilibrium. In spring, SAS1A showed more frequent and complete mixing events, with oxygen values rising to near 100% saturation in early June, while SAS2A never rose above ca. 30%. Lake SAS1A would therefore appear to be well mixed in fall and to a lesser extent in spring, while SAS2A is poorly mixed in both seasons, but especially in spring. These differences are likely related to differences in morphometry: SAS1A has a shallower relative depth (lower maximum depth/average fetch ratio; Table 1) and a longer fetch of 28 m versus 11.5 m for SAS2A that would favor wind-induced mixing, while SAS2A and the other SAS2 lakes have higher relative depth characteristics that would resist mixing (Lewis, 1983). The ratio of depth to fetch is also incorporated in the Wedderburn Number as a measure of thermocline tilting and potential for wind-induced mixing. Wedderburn calculations for a small (but less colored) thermokarst lake at a more northern latitude have shown how values for this parameter remained above 1 for much of summer, indicating resistance to mixing, but

with much lower values during fall that were indicative of mixing due to the breaking of nonlinear internal waves (Deshpande et al., 2015).

These observations imply that the timing and extent of release of GHG reserves stored beneath winter ice varies greatly among lakes, even in the same region and experiencing the same climate. In the Swedish subarctic lake study reported by Jammet et al. (2015), spring methane fluxes accounted for 53% of the total annual emissions, but in the peatland lakes studied here, the spring contribution may be less and variable. This variation may be controlled in part by lake fetch and depth as well as interannual fluctuations in climate, and such effects should be examined in replicate lakes over a broader range of morphometries.

The spring overturn in shallow lakes such as SAS1A and SAS1B is likely accompanied by a large outgassing from these lakes of CH_4, which may accumulate under the seasonal ice to over 400% of the corresponding average summer amount of 72 mmol CH_4 m^{-2} (Table 3). In deeper lakes such as SAS2A, only the gas stored in surface waters during winter may escape to the atmosphere. Due to this incomplete mixing in spring, most of the methane accumulated below the thermocline cannot evade at the breaking up of the ice, and is locked at the bottom by rapid development of the summer stratification. Thus, accumulation continues throughout the open water season and may reach oversaturation, potentially forming gas microbubbles that later contribute towards evasion (Matveev et al., 2016). The bottom waters will maintain a strongly reducing environment and will continue to accumulate CH_4 until more complete mixing of the lake occurs at the end of the open water season. We therefore surmise that the late autumn mixing period is likely to be a time of intense GHG emissions from the deeper thermokarst lakes of this subarctic region, requiring direct measurements in the future.

Methane concentrations in the near surface waters of lakes are determined by the balance between methanogenesis and two CH_4 loss processes: efflux to the atmosphere and

methanotrophy. This latter process in known to occur in anoxic as well as oxygenated environments (Oswald et al., 2016), including in subarctic lakes (Martinez-Cruz et al., 2017). Consistent with these observations, molecular microbiological studies have shown the presence of methane oxidation potential (specifically RNA transcripts of the gene coding for the pmoA subunit of the methane oxidizing enzyme) in both aerobic and anaerobic strata in these lakes (Crevecoeur et al., 2017). The results presented here show that methane can accumulate for prolonged periods of time, either under the ice during winter or in deep hypolimnetic waters during summer stratification. Both of these conditions provide increased time and opportunities for CH_4 consumption. It is therefore to be expected that methanotrophic bacteria account for a large fraction of total bacterial sequences in the analyses of samples from these waters (up to 27%; Crevecoeur et al., 2015), and their activity likely reduces CH_4 emissions while increasing that of CO_2.

5. Conclusions

Despite the increased attention to the biogeochemical properties of thermokarst lakes in recent years, much of this research has been restricted to yedoma-type permafrost regions and to sites in close proximity to well-established research facilities, such as in southern Alaska, northern Sweden, and parts of northern Russia. Lakes in other permafrost regions, including peatland thermokarst with a much higher carbon content relative to yedoma-type permafrost (Hugelius et al., 2013), have received less attention, partly because of the difficulty of access. For similar reasons, the winter CH_4 and CO_2 dynamics remain largely enigmatic for most thermokarst lake types. Our observations here for peatland permafrost thaw lakes in subarctic Quebec show that winter CH_4 and CO_2 concentrations are high in winter, and that the gases are homogenously distributed throughout the below ice water column, in contrast to the sharp gradients with depth in summer. Both gases also occur in the

lake ice, thus creating a potential for spring emissions from ice melt; however, this efflux is likely to be small compared to the potential break up-associated emissions from the underlying waters given their extreme supersaturation in CH_4 and CO_2.

The timing of full release of the gases that have accumulated under the ice is likely to be variable and dependent on mixing regime, in turn dependent on lake morphometry. In deeper lakes with a small wind fetch, mixing is incomplete in spring. Subsequently, CH_4 rises to higher concentrations in the bottom waters during summer, with full release more likely in fall, especially during years of more intense cooling and wind stress. However, in shallower lakes with larger wind fetch, much of the under-ice accumulation may be released during mixing in spring. To accurately estimate the annual evasion of CH_4 and CO_2 from thermokarst lakes will require attention not only to the summer diffusive flux (and ebullition flux), but also to winter storage and to fluxes during the fall and spring shoulder periods immediately before and after winter ice cover. This complete seasonal coverage is required for upscaling, modeling and reliable estimates of the Arctic carbon balance.

Acknowledgments

We acknowledge funding support from the Natural Sciences and Engineering Research Council of Canada (NSERC), the Canada First Excellence Research Fund (CFREF) program Sentinel North (specifically the project BOND led by Réal Vallée), the Canada Research Chair program, the Networks of Centres of Excellence program ArcticNet, and the Fonds de Recherche du Québec-Nature et Technologies (FRQNT) for funding to Centre d'études nordiques (CEN). We are also grateful to the management of the Whapmagoostui-Kuujjuarapik CEN station, the pilots of Canadian Helicopter Ltd., Martin Pilote (Environment and Climate Change Canada) for his valuable help in the field and two reviewers for their insightful comments and advice on the draft manuscript. All imagery,

climate and limnological datasets are made available via the northern data repository Nordicana D (http://www.cen.ulaval.ca/nordicanad/).

References

Abnizova, A., Siemens, J., Langer, M. & Boike, J. (2012), Small ponds with major impact: The relevance of ponds and lakes in permafrost landscapes to carbon dioxide emissions. *Global Biogeochemical Cycles*, 26, GB2041. https://doi.org/10.1029/2011GB004237

Arp, C.D., & Jones, B. M. (2009), Geography of Alaska lake districts: Identification, description and analysis of lake-rich regions of a diverse and dynamic state. *Reports*, 40 pp., U.S. Geological Survey, Reston, VA.

Arp, C.D., Jones, B.M., Grosse, G., Bondurant, A.C., Romanovsky, V.E., Hinkel, K.M., & Parsekian, A.D. (2016), Threshold sensitivity of shallow Arctic lakes and sublake permafrost to changing winter climate. *Geophysical Research Letters*, 43, 6358-6365. https://doi.org/10.1002/2016GL068506

Bastviken, D., Persson, L., Odham, G., & Tranvik, L. (2004), Degradation of dissolved organic matter in oxic and anoxic lake water. *Limnology and Oceanography*, 49, 109-116. https://doi.org/10.4319/lo.2004.49.1.0109

Bhiry, N., Delwaide, A., Allard, M., et al. (2011), Environmental change in the Great Whale River Region, Hudson Bay: Five decades of multidisciplinary research by Centre d'études nordiques (CEN). *Ecoscience*, 18, 182-203. https://doi.org/10.2980/18-3-3469

Breton, J., Vallières, C., & Laurion, I. (2009), Limnological properties of permafrost thaw ponds in northeastern Canada. *Canadian Journal of Fisheries and Aquatic Science*, 66, 1635-1648. https://doi.org/10.1139/F09-108

Chadburn, S. E., Burke, E. J., Cox, P. M., Friedlingstein, P., Hugelius, G., & Westermann, S. (2017), An observation-based constraint on permafrost loss as a function of global warming. *Nature Climate Change*, 7, 340. https://doi.org/10.1038/nclimate3262

Chaudhary, N., Miller, P. A., and Smith, B. (2017), Modelling past, present and future peatland carbon accumulation across the pan-Arctic region. *Biogeosciences*, 14, 4023-4044. https://doi.org/10.5194/bg-14-4023-2017

Crevecoeur, S., Vincent, W. F., Comte, J., & Lovejoy, C. (2015), Bacterial community structure across environmental gradients in permafrost thaw ponds: Methanotroph-rich ecosystems. *Frontiers in Microbiology*, 6, 192. https://doi.org/10.3389/fmicb.2015.00192

Crevecoeur, S., Vincent, W. F., Comte, J., Matveev, A., & Lovejoy, C. (2017), Diversity and potential activity of methanotrophs in high methane-emitting permafrost thaw ponds. *PLoS ONE*, 12, 1-22. https://doi.org/10.1371/journal.pone.0188223

Cunada, C. L., Lesack, L. F. W., & Tank, S. E. (2018), Seasonal dynamics of dissolved methane in lakes of the Mackenzie Delta and the role of carbon substrate quality. *Journal of Geophysical Research: Biogeosciences*, 123, 591-609. https://doi.org/10.1002/2017JG004047

Denfeld, B. A., Baulch, H. M., del Giorgio, P. A., Hampton, S. E., & Karlsson, J. (2018), A synthesis of carbon dioxide and methane dynamics during the ice-covered period of northern lakes. *Limnology and Oceanography Letters*, 3, 117-131. https://doi.org/10.1002/lol2.10079

Deshpande, B. N., Crevecoeur, S., Matveev, A., & Vincent, W. F. (2016), Bacterial production in subarctic peatland lakes enriched by thawing permafrost. *Biogeosciences*, 13, 4411-4427. https://doi.org/10.5194/bg-13-4411-2016

Deshpande, B. N., MacIntyre, S., Matveev, A., & Vincent W. F. (2015), Oxygen dynamics in permafrost thaw lakes: Anaerobic bioreactors in the Canadian subarctic. *Limnology and Oceanography*, 60, 1656-1670. https://doi.org/10.1002/lno.10126

Deshpande, B. N., Maps, F., Matveev, A., & Vincent, W. F. (2017), Oxygen depletion in subarctic peatland thaw lakes. *Arctic Science*, 3, 406-428. https://doi.org/10.1139/AS-2016-0048

Fillion, M.-È., Bhiry, N., & Touazi, M. (2014), Differential development of two palsa fields in a peatland located near Whapmagoostui-Kuujjuarapik, Northern Québec, Canada. *Arctic, Antarctic and Alpine Research*, 46, 40-54. https://doi.org/10.1657/1938-4246-46.1.40

Grant, R. F., Humphreys, E. R., & Lafleur, P. M. (2015), Ecosystem CO_2 and CH_4 exchange in a mixed tundra and a fen within a hydrologically diverse arctic landscape: 1. Modeling versus measurements. *Journal of Geophysical Research: Biogeosciences*, 120, 1366-1387. https://doi.org/10.1002/2014JG002888

Grosse, G., Jones, B. & Arp, C. (2013), 8.21 Thermokarst lakes, drainage, and drained basins. *In* Treatise on Geomorphology. J. F. Shroder [ed.], pp. 325-353. Academic Press, San Diego. https://doi.org/10.1016/B978-0-12-374739-6.00216-5

Grosse, G., Goetz, S., McGuire, A. D., Romanovsky, V. E., & Schuur, E. A. G. (2016), Changing permafrost in a warming world and feedbacks to the Earth system. *Environmental Research Letters*, 11: 040201. https://doi.org/10.1088/1748-9326/11/4/040201

Hampton, S. E., Moore, M. V., Ozersky, T., Stanley, E. H., Polashenski, C. M., & Galloway, A. W. (2015), Heating up a cold subject: prospects for under-ice plankton research in lakes, *Journal of Plankton Research*, 37, 277-284. https://doi.org/10.1093/plankt/fbv002

Hampton, S. E., et al. (2017), Ecology under lake ice. *Ecology Letters*, 20, 98-111. https://doi.org/10.1111/ele.12699.

Holgerson, M.A., & Raymond, P.A. (2016), Large contribution to inland water CO_2 and CH_4 emissions from very small ponds. *Nature Geoscience*, 9, 222-226. https://doi.org/10.1038/ngeo2654

Hugelius G., Strauss, J. , Zubrzycki, S., Harden, J. W., Schuur, E. A. G. , Ping, C., Schirrmeister, L., Grosse, G., & Michaelson, G. J. (2014), Estimated stocks of circumpolar permafrost carbon with quantified uncertainty ranges and identified data gaps. *Biogeosciences*, 11, 6573-6593. https://doi.org/10.5194/bg-11-6573-2014

Jammet, M., Crill, P., Dengel, S., & Friborg, T. (2015). Large methane emissions from a subarctic lake during spring thaw: Mechanisms and landscape significance. *Journal of Geophysical Research: Biogeosciences*, 120, 2289-2305. https://doi.org/10.1002/2015JG003137

Jammet, M., Dengel, S., Kettner, E., Parmentier, F.-J. W., Wik, M., Crill, P., & Friborg, T. (2017). Year-round CH_4 and CO_2 flux dynamics in two contrasting freshwater ecosystems of the subarctic. *Biogeosciences*, 14, 5189-5216. https://doi.org/10.5194/bg-14-5189-2017

Jones, B. M., Grosse, G., Arp, C. D., Jones, M. C., Walter Anthony, K. M., & Romanovsky, V. E. (2011), Modern thermokarst lake dynamics in the continuous permafrost zone, northern Seward Peninsula, Alaska. *Journal of Geophysical Research*, 116, G00M03. https://doi.org/10.1029/2011JG001666

Karlsson, J., R. Giesler, J. Persson, & E. Lundin (2013), High emission of carbon dioxide and methane during ice thaw in high latitude lakes, *Geophysical Research Letters*, 40, 1123-1127, https://doi.org/10.1002/grl.50152

Langer, M., Westermann, S., Walter Anthony, K., Wischnewski, K., & Boike, J. (2015), Frozen ponds: production and storage of methane during the Arctic winter in a lowland tundra landscape in northern Siberia, Lena river delta. *Biogeosciences*, 12, 977-990. https://doi.org/10.5194/bg-12-977-2015

Laurion, I., Vincent, W. F., MacIntyre, S., Retamal, L., Dupont, C., Francus, P., & Pienitz, R. (2010), Variability in greenhouse gas emissions from permafrost thaw ponds. *Limnology and Oceanography*, 55, 115-133. https://doi.org/10.4319/ lo.2010.55.1.0115

Livingstone, D. A., Bryan, K., & Leahy, R. G. (1958), Effects of an arctic environment on the origin and development of freshwater lakes. *Limnology and Oceanography*, 3, 192-214. https://doi.org/10.4319/lo.1958.3.2.0192

MacIntyre, S., Cortés, A., & Sadro, S. (2018). Sediment respiration drives circulation and production of CO_2 in ice-covered Alaskan arctic lakes. *Limnology and Oceanography Letters*, 3, 302-310. https://doi.org/10.1002/lol2.10083

Martinez-Cruz, K., Sepulveda-Jauregui, A., Walter Anthony, K., & Thalasso, F. (2015), Geographic and seasonal variation of dissolved methane and aerobic methane oxidation in Alaskan lakes. *Biogeosciences*, 12, 4595-4606. https://doi.org/10.5194/bg-12-4595-2015

Matveev, A., Laurion, I., & Vincent, W. F. (2018), Methane and carbon dioxide emissions from thermokarst lakes on mineral soils. *Arctic Science*, 4, 584-604. https://doi.org/10.1139/as-2017-0047

Matveev, A., Laurion, I., Deshpande, B. N., & Vincent, W. F. (2019), Concentrations of dissolved methane, carbon dioxide and oxygen in thermokarst lakes and ponds in palsa peatlands, northern Québec, Canada, v. 1.0 (2013-2016). *Nordicana*, D48, https://doi.org/ 10.5885/45588CE-5A12A84DFAAF4D36.

Matveev, A., Laurion, I., Deshpande, B. N., Bhiry, N., & Vincent, W. F. (2016), High methane emissions from thermokarst lakes in subarctic peatlands. *Limnology and Oceanography*, 61(S1), S150-S164. https://doi.org/10.1002/lno.10311

Michmerhuizen, C. M., Striegl R. G., & McDonald M. E. (1996), Potential methane emission from north-temperate lakes following ice melt, *Limnology and Oceanography*, 41, 985-991. https://doi.org/10.4319/lo.1996.41.5.0985

Morgenstern, A., Grosse, G., Günther, F., Fedorova, I., & Schirrmeister, L. (2011), Spatial analyses of thermokarst lakes and basins in yedoma landscapes of the Lena delta, *The Cryosphere*, 5, 849-867. https://doi.org/10.5194/tc-5-849-2011

Negandhi, K., Laurion, I., Whiticar, M. J., Galand, P. E., Xu, X., & Lovejoy, C. (2013), Small thaw ponds: An unaccounted source of methane in the Canadian High Arctic. *PLoS ONE*, 8, e78204. https://doi.org/10.1371/journal.pone.0078204

Olefeldt, D., Goswami, S., Grosse, G., Hayes, D., Hugelius, G., Kuhry, P., & Turetsky, M. R. (2016), Circumpolar distribution and carbon storage of thermokarst landscapes. *Nature Communications*, 7: 13043. https://doi.org/10.1038/ncomms13043

Oswald, K., Milucka, J., Brand, A., Hach, P., Littmann, S., Wehrli, B., Kuypers, M. M., & Schubert, C. J. (2016), Aerobic gammaproteobacterial methanotrophs mitigate methane emissions from oxic and anoxic lake waters. *Limnology and Oceanography*, 61(S1), S101-S118. https://doi.org/10.1002/lno.10312

Pienitz, R., Bouchard, F., Narancic, B., Vincent, W. F., & Sarrazin, D. (2017), Seasonal ice cover and catchment changes at northern thermokarst ponds in Nunavik: Observations from automated time-lapse cameras, v. 1.0 (2014-2015). *Nordicana D24*. https://doi.org/10.5885/45418AD-AF6A8064C702444B

Powers, S. M. & Hampton, S. E. (2016), Winter limnology as a new frontier. *Limnology and Oceanography Bulletin*, 25, 103-108. https://doi.org/10.1002/lob.10152

Riçao Canelhas, M., Denfeld, B. A., Weyhenmeyer, G. A., Bastviken, D., & Bertilsson, S. (2016), Methane oxidation at the water-ice interface of an ice-covered lake. *Limnology and Oceanography*, 61(S1), S78-S90. https://doi.org/10.1002/lno.10288

Saunois, M. et al. (2016), The global methane budget 2000-2012. *Earth System Science Data*, 8, 697-751. https://doi.org/10.5194/essd-8-697-2016

Serikova, S., Pokrovsky, O. S., Laudon, H., Krickov, I. V., Lim, A. G., Manasypov, R. M., & Karlsson, J. (2019), High carbon emissions from thermokarst lakes of Western Siberia. *Nature Communication*s, 10, 1552. https://doi.org/10.1038/s41467-019-09592-1

Schirrmeister, L., Froese, D., Tumskoy, V., Grosse, G., & Wetterich, S. (2013), Yedoma: Late Pleistocene ice-rich syngenetic permafrost of Beringia, / S. Elias, C. Mock and J. Murton [eds.], *Encyclopedia of Quaternary Science*, 3, 542-552. https://doi.org/10.1016/B978-0-444-53643-3.00106-0

Schneider von Deimling, T., Grosse, G., Strauss, J., Schirrmeister, L., Morgenstern, A., Schaphoff, S., Meinshausen, M., & Boike, J. (2015), Observation-based modelling of permafrost carbon fluxes with accounting for deep carbon deposits and thermokarst activity. *Biogeosciences*, 12, 3469-3488. https://doi.org/10.5194/bg-12-3469-2015

Townsend-Small, A., Åkerström, F., Arp, C. D., & Hinkel, K. M. (2017). Spatial and temporal variation in methane concentrations, fluxes, and sources in lakes in Arctic Alaska. *Journal of Geophysical Research: Biogeosciences*, 122, 2966-2981. https://doi.org/10.1002/2017JG004002

Utsumi M., Nojiri, Y., Nakamura, T., Nozawa, T., Otsuki, A., Takamura, N., Watanabe, M., & Seki, H. (1998), Dynamics of dissolved methane and methane oxidation in dimictic Lake Nojiri during winter. *Limnology and Oceanography*, 43, 1939-5590. https://doi.org/10.4319/lo.1998.43.1.0010

Vigneron, A., Lovejoy, C., Cruaud, P., Kalenitchenko D., Culley, A., & Vincent, W.F. (2019), Contrasting winter versus summer microbial communities and metabolic functions in a permafrost thaw lake. *Frontiers in Microbiology*, 10.1656. https://doi.org/10.3389/fmicb.2019.01656

Vincent, W. F., Lemay, M., &Allard, M. (2017), Arctic permafrost landscapes in transition: towards an integrated Earth system approach. *Arctic Science*, 3, 39-64. https://doi.org/10.1139/as-2016-0027

Vincent, W. F., Laurion, I., Pienitz, R., & Walter Anthony, K. M. (2013), Climate impacts on Arctic lake ecosystems, p.27-42. *In*: C. R. Goldman, M. Kumagai, and R. D. Robarts [eds.], Climatic change and global warming of inland waters: Impacts and mitigation for ecosystems and societies. Wiley, https://doi.org/10.1002/9781118470596.ch2

Vonk, J.E., Tank, S. E., Bowden, W. B., et al. (2015), Effects of permafrost thaw on Arctic aquatic ecosystems. *Biogeosciences*, 12, 7129-7167. https://doi.org/10.5194/bg-12-7129-2015

Watanabe, S., Laurion, I., Pienitz, R., Chokmani, K., & Vincent, W. F. (2011), Optical diversity of thaw ponds in discontinuous permafrost: A model system for water color analysis. *Journal of Geophysical Research*, 116, G02003 https://doi.org/10.1029/2010JG001380

Wauthy, M., Rautio, M., Christoffersen, K. S., Forsström, L., Laurion, I., Mariash, H., Peura, S., & Vincent, W. F. (2018), Increasing dominance of terrigenous organic matter in circumpolar freshwaters due to permafrost thaw. *Limnology and Oceanography*, 3, 186-198. https://doi.org/10.1002/lol2.10063

Wetzel, R. G. and G. Likens. 2002. Limnological Analyses. Springer-Verlag New York, 3rd edition. https://doi.org/10.1007/978-1-4757-3250-4

Wik, M., Thornton, B. F., Bastviken, D., Uhlbäck, J., & Crill, P. M. (2016b), Biased sampling of methane release from northern lakes: A problem for extrapolation. *Geophysical Research Letters*, 43, 1256-1262. https://doi.org/10.1002/ 2015GL066501

Wik, M., Varner, R. K., Walter Anthony, K., MacIntyre, S., & Bastviken, D. (2016a), Climate-sensitive northern lakes and ponds are critical components of methane release. *Nature Geosciences*, 9, 99-105. https://doi.org/10.1038/ngeo2578

Wrona, F. J., Johansson, M., Culp, J. M., Jenkins, A., Mård, J., Myers-Smith, I. H., Prowse, T. D., Vincent, W. F., & Wookey, P. A. (2016), Transitions in Arctic ecosystems: Ecological implications of a changing hydrological regime. *Journal of Geophysical Research: Biogeosciences*, 121, 650-674. https://doi.org/10.1002/2015JG003133

Zimov, S. A., Voropaev, Y.V., Semiletov, I. P., Davidov, S., Prosiannikov, S., Chapin III, F. S., Chapin, M.C., Trumbore, S. & Tyler, S. (1997), North Siberian lakes: A methane source fueled by Pleistocene carbon. *Science*, 277, 800-802. https://doi.org/10.1126/science.277.5327.800

Table 1. Localization and morphometric properties of the peatland thermokarst lakes in the SAS study region.

Lake	Area (m^2)	Maximum depth (m)	Relative depth* (%)	Approximate surface shape	Latitude (ºN)	Longitude (ºW)
SAS1A	1580	1.8	4.0	lunate	55.218800	77.707950
SAS1B	175	1.4	9.4	dendritic	55.219013	77.707801
SAS2A	196	2.8	17.7	circular	55.225018	77.696580
SAS2B	134	2.1	16.1	circular	55.225212	77.696017
SAS2C	182	2.2	14.5	subcircular	55.225083	77.694933

*Relative depth (Z_r), calculated as in *Wetzel and Likens* (2002) as $Z_r = 100 Z_{max}/F$, where Z_{max} is the maximum depth and F is the average fetch, estimated as $2\pi^{-1/2}A^{1/2}$ (the diameter of a circular lake of same area A). Larger values imply less wind-induced mixing.

Table 2. Snow, ice and atmospheric conditions at the study sites during the March 2016 sampling.

Lake	Date (2016)	Air Temp. (ºC)	Atm. Pressure (hPa)	Wind (m s^{-1})	Snow depth (m)	Snow description	Ice depth (m)	Notes
SAS2A	19.03	–21.6	1001.8	3.8	0.48	semi-light, grained, wet near the ice	0.57	water over ice, 0.07 m
SAS2B	20.03	–23.4	998.9	4.1	0.50	semi-light, grained, wet near the ice	0.56	water over ice, 0.06 m
SAS2C	21.03	–21.2	1000.5	4.5	0.48	semi-light, grained near the ice	0.58	dry ice
SAS1A	22.03	–22.9	997.3	4.7	0.53	light, light grains, pack near the ice	0.58	dry ice
SAS1B	23.03	–23.5	1004.4	5.3	0.52	light, light grains	0.63	dry ice

Table 3. Average winter and summer concentrations and the total amount of dissolved gas accumulated in the unit water column (Total gas*) of lakes by site, and % difference between its winter and summer accumulations relative to summer (% difference).

Lake	Winter		Summer		'Total gas'
	Concentration (mmol m^{-3})	Total gas* (mmol m^{-2})	Concentration (mmol m^{-3})	Total gas* (mmol m^{-2})	Difference (%)
CH_4					
SAS1A	318	312	34	64	388
SAS1B	160	85	53	80	6
SAS2A	208	344	115	299	15
SAS2B	183	266	101	261	2
SAS2C	211	294	109	282	4
CO_2					
SAS1A	1349	1369	541	1054	30
SAS1B	1344	842	1392	2081	–60
SAS2A	2769	4521	2519	6750	–33
SAS2B	2363	3417	2030	5181	–34
SAS2C	1975	2775	1554	4000	–31

* The total amount of dissolved gas accumulated in the unit water column ('Total gas') calculated in the lake water column with 1 m^2 surface area assuming uniform concentrations within each measured depth layer of 0.1-0.2 m, and integrated from surface (summer) and from below the ice (winter) to the lake bottom.

Table 4. Gas trapped in the ice (winter 2015-2016): concentrations measured in melt water from the top 0.3 m of the lake ice, and the total amount of dissolved gas accumulated in the unit water column ('Total gas'* - see Table 3) calculated for the total lake ice column assuming uniform gas concentrations throughout. Ice 'Total gas' accumulations are given as % of winter stocks in the water column.

Lake				Ice 'Total gas' (mmol m^{-2})		Water 'Total gas' (mmol m^{-2})		% ice ('Total gas'	
	CO_2 (µM)	CH_4 (µM)	Ice depth (m)	CH_4	CO_2	CH_4	CO_2	CH_4	CO_2
SAS2A	62	10	0.57	6	35	344	4521	1.7	0.8
SAS2C	317	13	0.58	7	184	294	2775	2.5	6.6
SAS1A	78	29	0.58	17	45	312	1369	5.4	3.3
SAS1B	42	<1	0.63	0.6	27	85	842	0.7	3.2

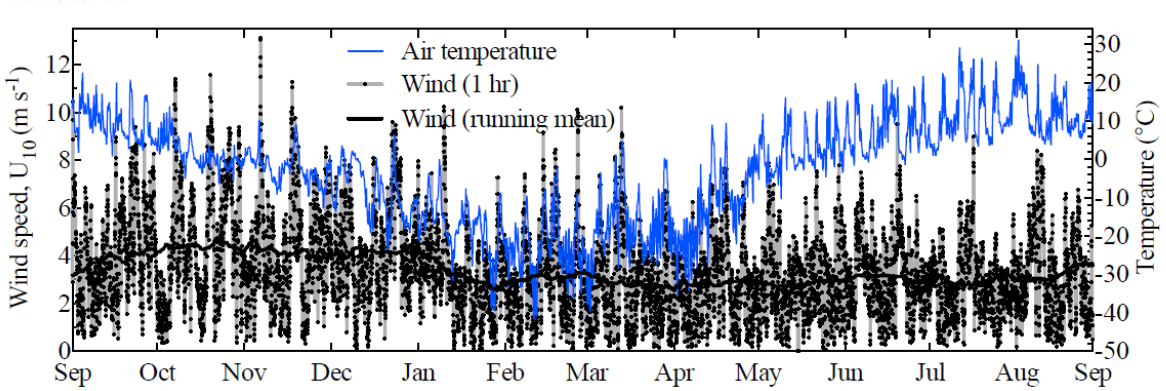

Figure 1. Air temperature (T in ºC, blue line) and wind speed (U_{10} in m s^{-1}, black dots for 1h-averages, black line for the running mean) measured at the CEN automated weather station (KJRAPIK.site#2, 8 km from the SAS valleys) between August 2015 and September 2016.

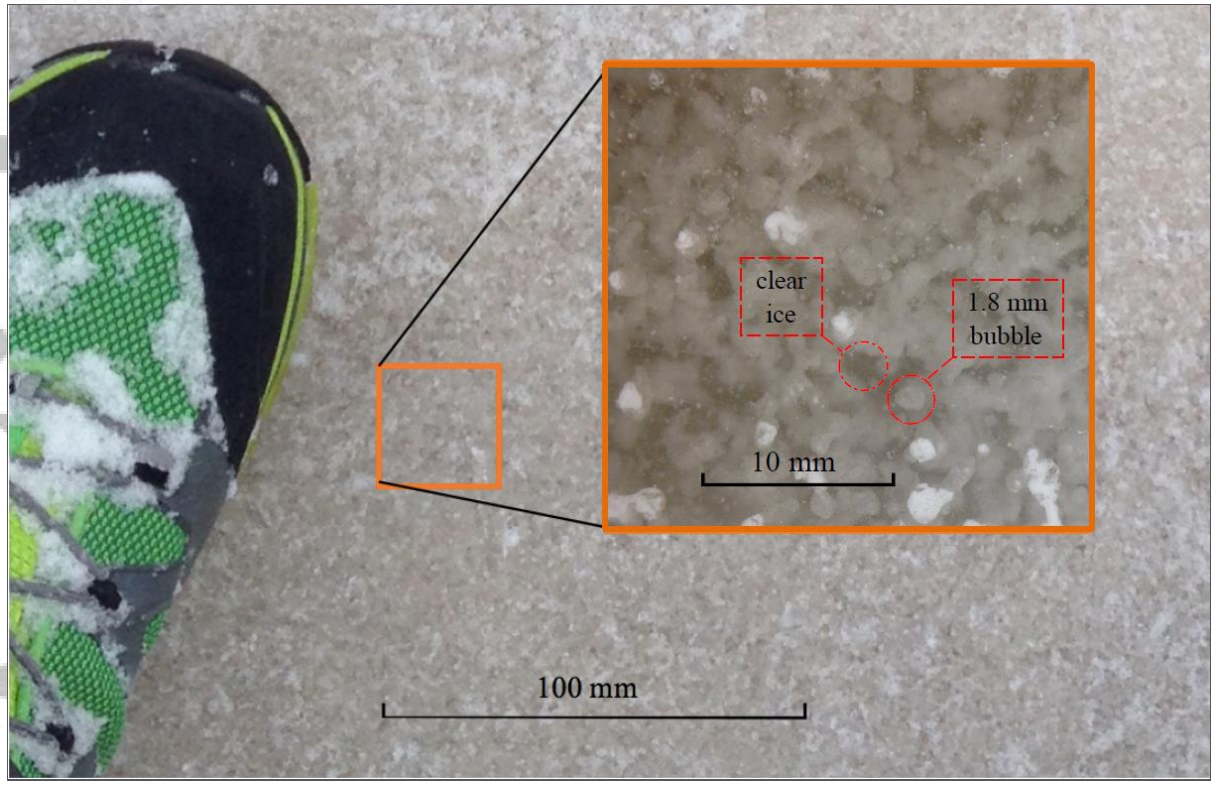

Figure 2. Small bubble inclusions (white and light grey) in the lake SAS2C ice (dark brown-grey) in March 2016.

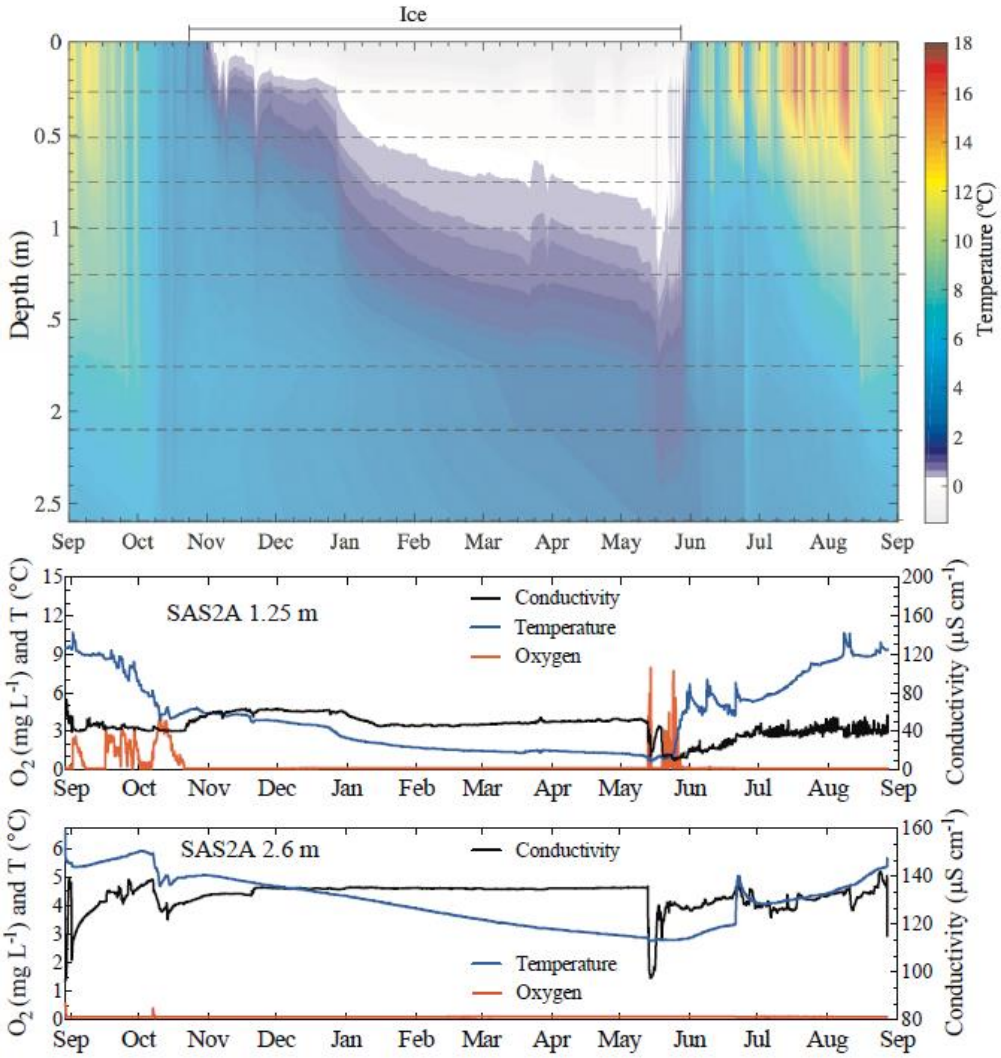

Figure 3. The annual variations in temperature, oxygen and conductivity measured in SAS2A, from 2015 to 2016. The ice period was determined by the automated camera record, with ice thickness (white area) inferred from the in situ thermistor records (the dashed lines mark the depths of the thermistors). The white shading corresponding to 0 ºC temperature (upper image) is based on the interpolated thermistor data with the uppermost sensor located at 0.25 m depth. Note the different scales used for middle (1.25 m) and bottom (2.6 m) waters. Expanded plots are given in Figure S5.

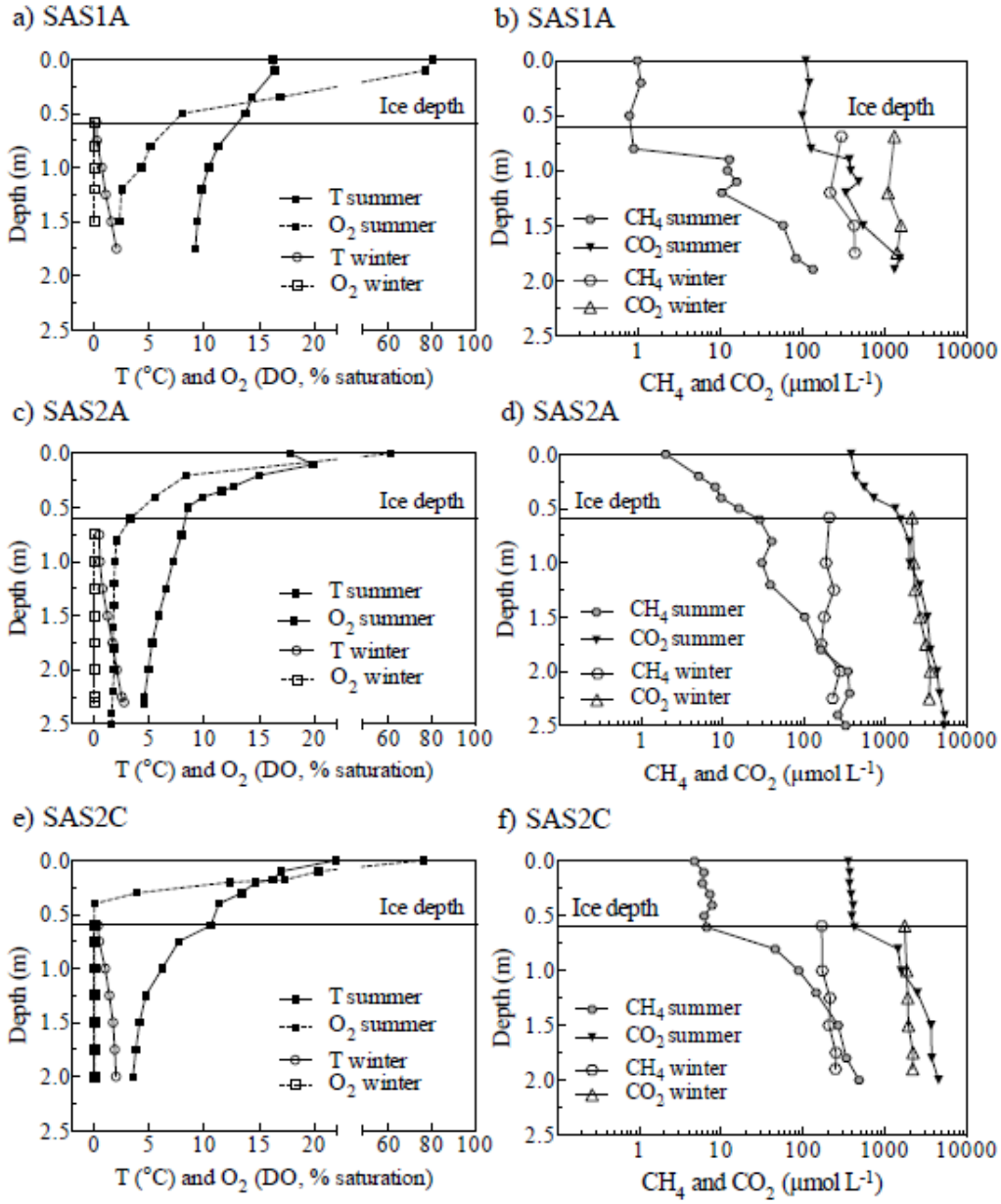

Figure 4. Summer 2014 or 2015 and winter 2016 profiles of temperature (T) and concentrations of dissolved O_2 (as % of the saturation value for water in equilibrium with air at the same temperature), CO_2 and CH_4 in the water column of lakes at in the SAS1 and SAS2 valleys. Additional profiles are given in Supporting Information Figure S6.

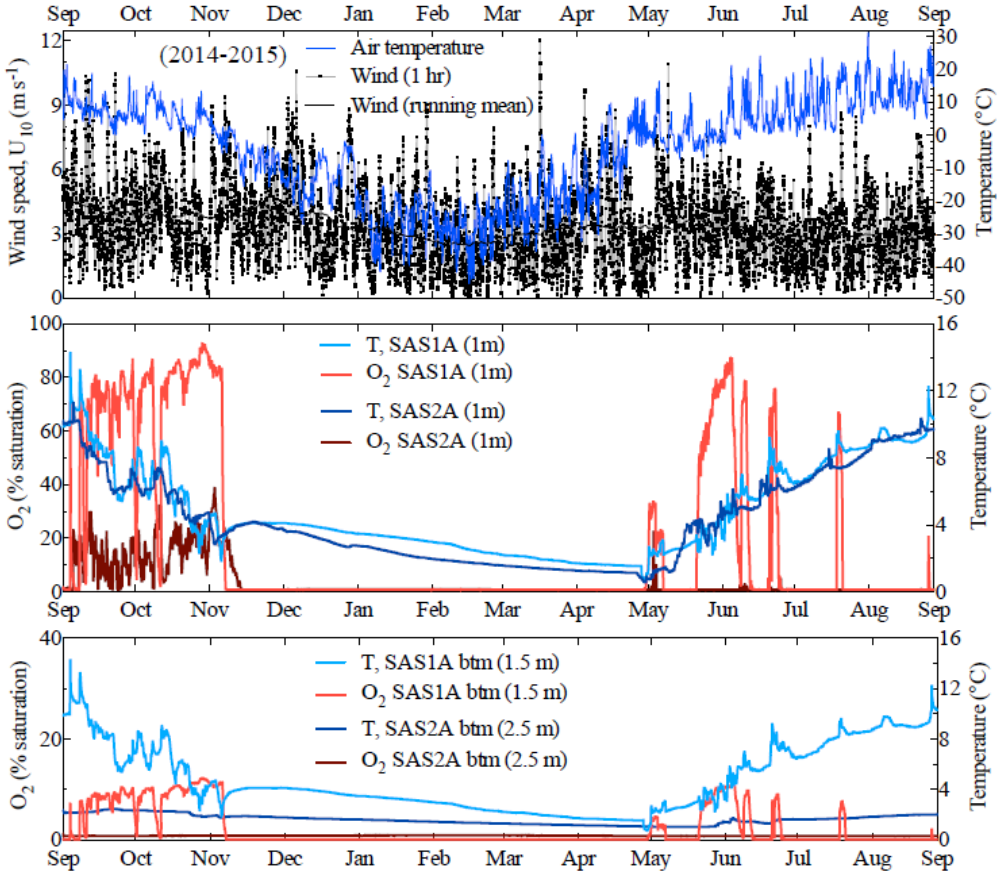

Figure 5. Air temperature (T in ºC, blue line) and wind speed (U10 in m s^{-1}, black dots for 1h-averages, black line for the running mean) measured at the CEN automated weather station (KJRAPIK.site#2, 8 km from the SAS valleys), and the annual variations in temperature, oxygen and conductivity measured in SAS2A between August 2014 and September 2015.